physica status solidi rrl
www.pss-rapid.com

Raman Spectroscopic Study of the Optical Phonons of $Mg_2Si_{1-x}Sn_x$ Solid Solutions

Mohammad Yasseri, Dominique Schüpfer, Limei Chen, Hasbuna Kamila, Eckhard Müller, Johannes de Boor, and Peter J. Klar**

$Mg_2Si_{1-x}Sn_x$ solid solutions are prepared in the composition range from $x = 0$ to 1 by mechanical alloying using high-energy ball milling followed by direct-current sintering at 600–800 °C. X-ray diffraction analysis confirms that the samples obtained are uniform solid solutions. Raman spectroscopy shows two first-order phonon Raman bands and a distribution of Raman signals due to second-order phonon Raman scattering. The first-order Raman bands are assigned to the nondegenerate Raman-forbidden F_{1u} (LO) mode and the triply degenerate Raman-allowed F_{2g} mode. Both modes exhibit a linear shift of the phonon frequency with a composition showing a clear one-mode behavior for this solid solution. The findings are discussed in the context of existing theories for the occurrence of the one-mode or two-mode behavior of phonons in solid solutions.

$Mg_2Si_{1-x}Sn_x$ solid solutions have attracted considerable attention in recent years in the field of thermoelectric materials.[1] Light weight, environmental compatibility, precursor abundance, and high thermoelectric performance ($zT \approx 1.1$–1.5) make these compounds attractive candidates for waste heat recovery.[1a,c] Ideally, a highly efficient thermoelectric material has a low thermal conductivity κ (which is governed by electronic and lattice contributions), a large absolute value of the Seebeck coefficient S, and a high electrical conductivity σ in the temperature range of interest, as the thermoelectric conversion efficiency is related to the dimensionless figure of merit $zT = S^2 \sigma T \kappa^{-1}$ where T is the absolute temperature.[2] The lattice thermal conductivity κ_L itself can be empirically described as $\kappa_L = C_V \bar{v}_g \bar{l}/3$, where C_V is the specific heat, $\bar{v}$ is the mean value of group velocity, and $\bar{l}$ is the phonon mean free path.[3] The substitution of Si by Sn in Mg_2X (X = Si, Sn) has been established as an efficient way to reduce the lattice thermal conductivity in the experiment.[1c,d]

Several effects may contribute to a reduction of the lattice thermal conductivity in alloys or solid solutions (such as $Mg_2Si_{1-x}Sn_x$ or $Si_{1-x}Ge_x$) compared with the corresponding binary crystalline compounds (such as Mg_2Si or Mg_2Sn) or elemental crystalline materials (such as Si or Ge). Typical contributions include enhanced phonon scattering induced by alloy disorder and tuning of the phonon dispersions (assuming that the virtual crystal approximation is valid), yielding a lower mean value of group velocity[1a,b,4] or the introduction of localized vibrational modes, as reported for $Si_{1-x}Ge_x$[5] or ZnO_xS_{1-x}.[6] The latter is typically reflected by the occurrence of a two-mode behavior of the optical phonons on alloying instead of a one-mode behavior. Thus, the subtleties of the phonon structure of the solid solution play a key role in determining the magnitude of the various contributions which may lead to a reduction in thermal conductivity in solid solutions compared with its compound or elemental counterparts. It is still difficult to predict the behavior of the optical phonons in alloys. There are rule of thumb models for predicting the one-mode and two-mode behavior of the optical phonons in solid solutions of the type $AB_{1-x}C_x$, but these are not always conclusive.[7] Ab initio calculations of the phonon structure, by either using the coherent potential approach or very large supercells, probably possess the best predictive power to distinguish between one- and two-mode behaviors but still may fail.[8]

Although there are many studies of the phonons of Mg_2X (X = Si, Ge, Sn) using first-principles theory[9] or Raman spectroscopy[10] or neutron scattering experiments,[11] experiments addressing the phonons in $Mg_2Si_{1-x}Sn_x$ solid solutions are still lacking. The first attempts of using ab initio theory for calculating the phonon properties of $Mg_2Si_{1-x}Sn_x$ solid solutions have been made.[4,12] Tan et al. also related the derived phonon dispersions with the thermal conductivity of the alloys in the framework of Boltzmann transport theory.[4] Here, we report on a first Raman

M. Yasseri, Prof. E. Müller
Institute of Inorganic and Analytical Chemistry
Justus Liebig University
Giessen DE- 35392, Germany
E-mail: Mohammad.Yasseri@dlr.de

M. Yasseri, H. Kamila, Prof. E. Müller, Dr. J. de Boor
Institute of Materials Research
Linder Hoehe, German Aerospace Center (DLR)
Koeln DE-51147, Germany

M. Yasseri, D. Schüpfer, Dr. L. Chen, Prof. E. Müller, Prof. P. J. Klar
Center for Materials Research/LaMa
Justus Liebig University
Heinrich-Buff-Ring 16, Giessen DE-35392, Germany
E-mail: Peter.J.Klar@exp1.physik.uni-giessen.de

D. Schüpfer, Dr. L. Chen, Prof. P. J. Klar
Institute of Experimental Physics I
Justus Liebig University
Heinrich-Buff-Ring 16, Giessen DE-35392, Germany

The ORCID identification number(s) for the author(s) of this article can be found under https://doi.org/10.1002/pssr.201900574.

DOI: 10.1002/pssr.201900574

study of the optical phonons of the $Mg_2Si_{1-x}Sn_x$ solid solutions and reveal a one-mode behavior on alloying. The investigation contributes to the understanding of the influence of solid-solution formation on the lattice thermal conductivity of $Mg_2Si_{1-x}Sn_x$ mixed crystals.

X-ray diffraction (XRD) results of $Mg_2Si_{1-x}Sn_x$ samples with $x = 0$, 0.15, 0.2, 0.4, 0.5, 0.6, 0.7, 0.8, 0.9, and 1.0 are shown in **Figure 1**. All samples of the solid solution crystallize in the antifluorite structure independent of composition x. The reflex positions are labelled according to the corresponding lattice planes. The linear shift of all reflex positions toward lower 2θ values is indicative of an increase in the lattice constant with increasing Sn content. The samples are polycrystalline and of high purity. However, the samples with $x = 0.4$, 0.5, and 0.6 have slightly broader (220) peaks than expected from alloy disorder, indicating that they are less homogeneous and probably exhibit a tendency toward phase segregation.[13]

The Raman spectra of $Mg_2Si_{1-x}Sn_x$ samples with $x = 0$, 0.15, 0.2, 0.4, 0.5, 0.6, 0.7, 0.8, 0.9, and 1.0 are shown in **Figure 2**. As discussed earlier, all members of the solid solution can be described to possess an antifluorite structure based on a face-centered cubic (fcc) lattice.[9a,10a] The primitive unit cell of the antifluorite structure contains three atoms yielding nine phonon branches. Three of them are assigned to the acoustic phonons (LA and TA) and six optical phonon branches. At the center of the Brillouin zone (wavevector $\boldsymbol{q} = 0$), group theory predicts two triply degenerate optical phonon modes. One of them is of F_{2g} symmetry and Raman active, whereas the other one is of F_{1u} symmetry and IR active. However, the degeneracy of the latter is lifted by the macroscopic Coulomb field due to the Fröhlich interaction and splits into a single F_{1u}(LO) mode and a doubly degenerate F_{1u}(TO) mode. Furthermore, according to a previous

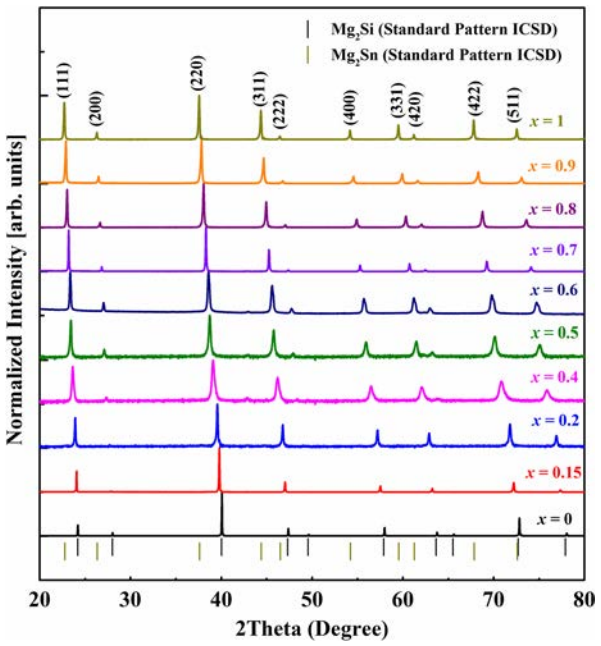

Figure 1. XRD patterns of $Mg_2Si_{1-x}Sn_x$ samples with $x = 0$, 0.15, 0.2, 0.4, 0.5, 0.6, 0.7, 0.8, 0.9, and 1.0, ball milled and sintered using the parameters given in Table 1.

study,[10b] the Fröhlich interaction induces Raman activity for the F_{1u} modes in the binary Mg_2X. The Fröhlich interaction may induce the Raman activity of modes that are Raman "forbidden" according to group symmetry, such as the ungerade modes in centrosymmetric crystals.[14] The Fröhlich interaction as an electron–phonon interaction may cause a change of the polarizability of the modes without electron–phonon interaction according to group theory so called ungerade modes.[14] This holds, in particular, for materials of a fluorite structure such as CaF_2, SrF_2, and BaF_2, in resonance with optical transitions such as the E_0 or E_1 gap and their spin–orbit split-off counterparts.[14] The same should also hold for polar materials of an antifluorite structure such as $Mg_2Si_{1-x}Sn_x$ solid solutions. Thus, the F_{1u}(LO) mode is typically observed in the Raman spectra of Mg_2X (X = Si, Ge, Sn) in addition to the F_{2g} mode.[10b] However, it cannot be ruled out that the Raman activity in the binaries and in particular in the solid solutions is induced by disorder, i.e., deviations of the real from the ideal structure, in the latter case due to alloy disorder. On the left graph of Figure 2, we focus on the spectral range of the one-phonon Raman signals between 200 and 400 cm^{-1}. The strongest mode in all spectra, shifting from about 260 to 220 cm^{-1}, with increasing x from 0 to 1, is assigned to the F_{2g} mode. For $x = 0.5$, 0.6, 0.7, and 0.8, this mode exhibits a line broadening and a certain asymmetry caused by alloy disorder. The weaker feature (highlighted by squares) that shifts from 350 to 240 cm^{-1}, increasing x from 0 and 1, is due to the F_{1u}(LO) mode. The intensity of the F_{1u}(LO) mode first increases with x up to 0.2 and then decreases again for a larger x. The reason may be that the excitation laser is, at $x = 0.2$, in resonance with the E_1 gap, which corresponds to direct transitions between the highest valence and the lowest conduction band along the Λ direction of the first Brillouin zone of the fcc lattice where the two bands shift parallel in energy. The second-order Raman spectrum of Mg_2Si as well as of Mg_2Sn differs for excitation above or below the E_1 gap.[10b] Assuming that the E_1 gap of the solid solution $Mg_2Si_{1-x}Sn_x$ varies continuously with composition x, between a value of about 2.6 eV for Mg_2Si and 2.2 eV for Mg_2Sn, it will be, at a specific x, in resonance with the laser excitation energy of 2.4 eV. At the crossing point (resonance), the appearance of the second-order Raman spectra in the series should switch rather abruptly. Assuming a linear dependence of the optical E_1 gap, this resonance should be at about $x \approx 0.5$. If additional bowing of the bandgap is present, x where the resonance occurs may be even smaller, e.g., $x \approx 0.2$. This is further corroborated by the appearance of a 3LO feature (at around 960 cm^{-1}) in the Raman spectrum of the sample with $x = 0.2$ at this excitation energy (2.4 eV). This 3LO signal is not visible when off-resonance excitation, e.g., 633 nm (1.96 eV), is used. The appearance of the 3LO signal at resonance with the E_1 gap is also a manifestation of a strong electron–phonon coupling which in turn is responsible for the Fröhlich interaction. The positions of the Raman modes F_{2g} and F_{1u}(LO) for Mg_2Si ($x = 0$) of 259 and 350 cm^{-1} are in good agreement with the literature.[10a-c,15] The same holds for the F_{2g} and F_{1u}(LO) mode positions of, respectively, 221 and 241 cm^{-1} in the Mg_2Sn ($x = 1$) spectrum.[10a,b,d,16]

The right graph shows the full spectral range between 100 and 1000 cm^{-1}. All Raman signals at wavenumbers larger than 400 cm^{-1} are related to two-phonon Raman processes. In a previous study,[10b] the Raman signals of Mg_2Si at 444 and 571 cm^{-1}

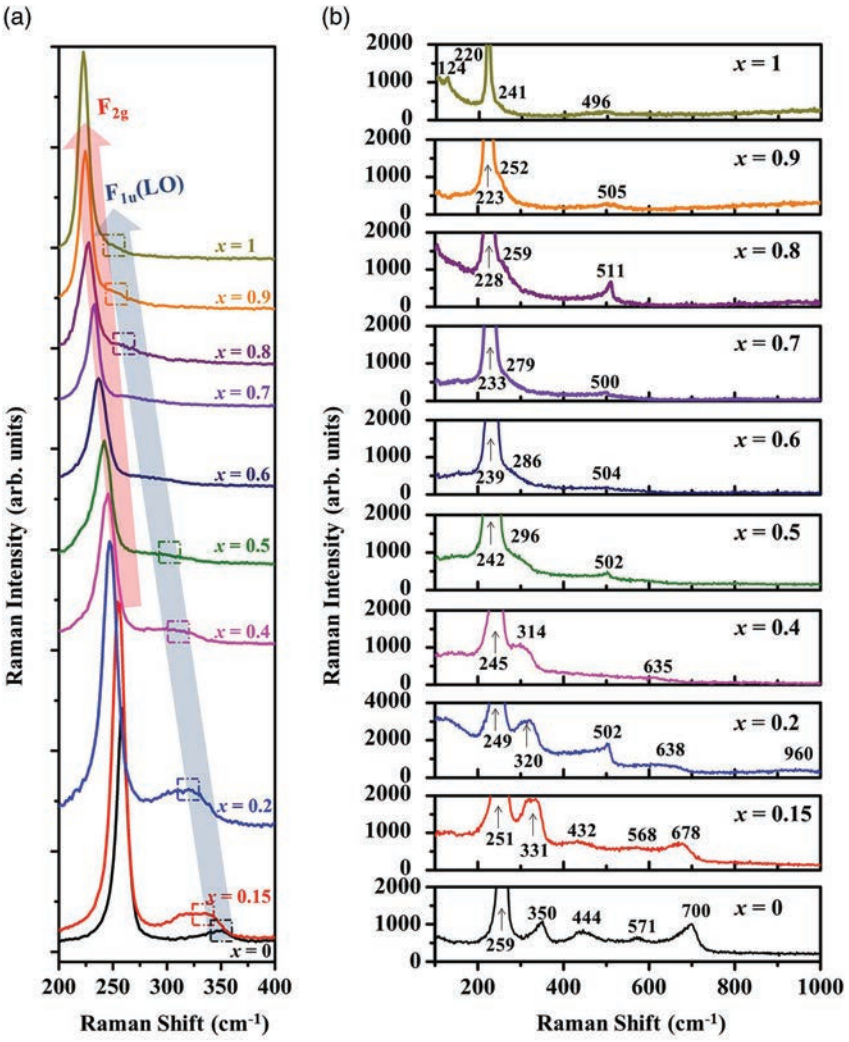

Figure 2. Raman spectra of $Mg_2Si_{1-x}Sn_x$ samples with $x = 0$, 0.15, 0.2, 0.4, 0.5, 0.6, 0.7, 0.8, 0.9, and 1.0 obtained with 514.5 nm excitation. a) The spectral region of one-phonon Raman signals. b) The full range with two-phonon Raman signals at wavenumbers larger than 400 cm^{-1}.

are assigned to $2F_{1g}$(LO) and $2F_{1u}$(TO) phonon branches out of the Γ point, whereas the origin of the peak at 700 cm^{-1} is the $2F_{1u}$(LO) process. They agree well with previously reported results.[10a-c,15] The additional Raman peak in the spectrum of the Mg_2Sn sample at 124 cm^{-1} is assigned to F_{1u}(TO) mode in the literature.[10a,b,d,16]

In **Figure 3**, the Raman shifts of the optical phonon modes of the $Mg_2Si_{1-x}Sn_x$ solid solutions are plotted versus Sn content x. The results indicate that for both phonons, F_{2g} and F_{1u}(LO), the Raman shift in $Mg_2Si_{1-x}Sn_x$ solid solutions varies linearly with x, exhibiting the following, $\omega(F_{2g}) = 259 - 38\ cm^{-1} \cdot x$ and $\omega(F_{1u}(LO)) = 348 - 106\ cm^{-1} \cdot x$, respectively. Such linear relationships for the variation of optical phonons with a composition are clear signatures of a one-mode behavior. This result is similar to the behavior observed in the cases of $Cd_{1-x}Pb_xF_2$, $Ca_{1-x}Sr_xF_2$, and $Sr_{1-x}Ba_xF_2$ crystals with fluorite structures, showing a one-mode behavior of optical phonons.[17]

In the following paragraphs, we would like to discuss our experimental findings in the light of existing theoretical results.

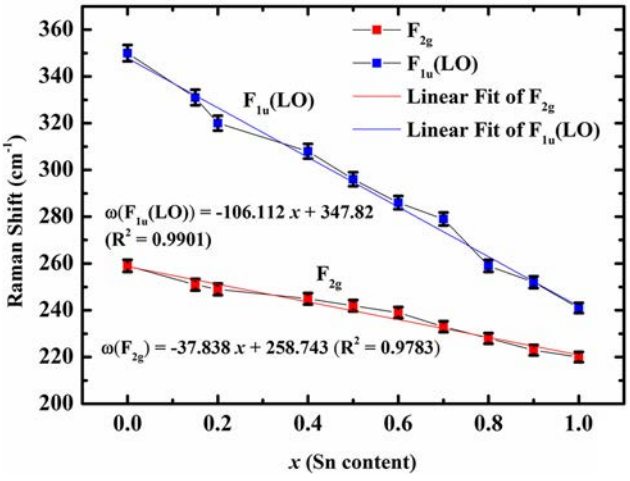

Figure 3. Raman shifts of the optical phonon modes of $Mg_2Si_{1-x}Sn_x$ compositions versus x. The linear fits of Raman shifts corresponding to F_{1u}(LO) and F_{2g} are denoted next to the respective curves.

In solid solutions, one distinguishes between the one-mode and two-mode behaviors of optical phonons. In case of one-mode behavior, as observed by us, the optical mode frequencies of $AB_{1-x}C_x$ solid solutions vary with composition x from one end member, AB, to the other, AC, with the modes keeping their extended mode character as longitudinal and transversal optical phonons. In contrast, in case of two-mode behavior, the local mode of impurities C occurs in host AB in the dilute limit and is converted with increasing x to the extended longitudinal and transversal modes resembling those of AC and vice versa for the local mode of impurities B in host AC with increasing $(1-x)$.[7b] Obviously, in case of two-mode behavior, the strength of the Raman and IR signals of phonon modes of solid solutions varies strongly with x.[7b] Empirical models have been developed between 1950 and 1970 for describing and predicting the mode behavior of solid solutions of the type $AB_{1-x}C_x$.[7a,b,18] The models are linear-chain models of binary host materials with two atoms per unit cell. Bjork accounted in his work for changes in the mass of the impurity as well as for a different force constant between host atoms and impurity.[7a] Lucovsky et al.[7c,18] suggested two criteria for the formation of localized or gap modes (two-mode behavior) in mixed crystals; the first is based on the bonding nature of the crystal, whether it is ionic or covalent (one-mode behavior is favored in case of an ionic nature) and the second considers the mass of substituted atoms in such solid solutions in comparison with that of the host atoms.[7b,18] A stronger condition is suggested by Chang and Mitra[7b] in their random-element-isodisplacement model, which accounts for changes in the reduced mass of atoms in the solid solution and for changes of the force constants between the atoms. It is worth noting that Lucovsky et al.[7c] reported a correct prediction of the mode behavior of ternary alloys in 18 out of 21 cases studied. The ternary solid solutions analyzed by them possessed host crystal structures of diamond, zincblende, or rocksalt structures, i.e., with two atoms as the basis in the primitive unit cell. For those three crystal structures, the vibrational modes propagating along the (111) direction can be well described by a diatomic chain model of atoms A and B as the corresponding mode patterns can be imagined as planes of atoms of type A vibrating against planes of atoms of type B. In case of $Mg_2Si_{1-x}Sn_x$, these models need to be treated cautiously as the antifluorite structure of Mg_2X has three atoms per primitive unit cell. However, when considering vibrations along the (100)-like directions, the antifluorite lattice of Mg_2Si (or Mg_2Sn) may be considered as consisting of alternating planes containing either Mg atoms or Si (or Sn) atoms. Taking into account that the planes consisting of Mg atoms contain twice the number of atoms than their Si (or Sn) counterparts, the situation may be to a first approximation described by a diatomic chain consisting of atoms of type A with atomic mass $M_A = 2M_{Mg} = 48$ u and type B with $M_B = M_{Si} = 24$ u (M_{Sn}) where type C with $M_C = M_{Sn} = 118$ u (M_{Si}) acts as impurity on B sites.

Lucovsky et al. distinguish four cases given by the criteria of whether M_A is larger or smaller than M_B and whether the parameter $\varepsilon = 1 - M_C/M_B$ is larger or smaller than zero.[7c] The quasidiatomic situation along (100) in the case of Mg_2Si:Sn corresponds to Lucovsky's case (c), where $M_A > M_B$ and $\varepsilon < 0$. In this case, (c), where the lighter atom of the host AB is replaced by a heavier atom C, no localized mode should occur at higher frequencies, but a gap mode may emerge at frequencies below the optical phonon bands of the host. The situation for Mg_2Sn:Si is case (b), where $M_A < M_C$ and $\varepsilon > 0$, which may exhibit two impurity-induced modes, a gap mode emerging from the top of the acoustic phonon bands and a local mode rising out of the top of the optical phonon band.

The model of Chang and Mitra states that a local mode B in AC exists, if the following inequality relationship holds, $M_B < \mu_{AC} < M_A$, M_C, where μ_{AC} is the reduced mass of M_A and M_C.[7b] Furthermore, a gap mode C in AB should exist, if $M_C > \mu_{AB}$ is fulfilled, where μ_{AB} is the reduced mass of M_A and M_B. Carrying out the calculus for Mg_2Si:Sn in the approximation of a diatomic chain along a (100) direction yields that both inequality relations are fulfilled, i.e., suggesting the existence of a local Si mode in Mg_2Sn as well as a gap mode of Sn in Mg_2Si. In contrast, the inequalities of Chang and Mitra cannot be fulfilled in case of Mg_2Sn:Si, suggesting no localized mode of Sn in Mg_2Si and no gap mode of Si in Mg_2Sn according to this model.

Thus, the two empirical models yield contradicting results. Furthermore, the predictions do not agree with our experimental findings. The likely reason for the failure of these models in describing the experiments is that the mode patterns of the diatomic chain do not match the situation in the primitive unit cell of the antifluorite structure with three atoms per cell. For example, in the case of the Raman-active F_{2g} mode, only the Mg atoms should vibrate and contribute to the mode pattern at wavevector $\boldsymbol{q} = 0$, whereas Sn or Si can be considered at rest[19], whereas in the primitive unit cell of the diatomic chain, the A and B atoms vibrate against each other at $\boldsymbol{q} = 0$ in case of the optical mode. A similar situation arises for the fluorite structure when alloying on the cation sublattice, e.g., in the case of $Ca_{1-x}Sr_xF_2$ or $(Cd,Pb)F_2$. The corresponding F_{2g} mode pattern is characterized by a stationary cation and the two fluorine atoms vibrating against each other.[20b] The theoretical models of the phonons of these solid solutions, which account for the specific mode patterns, yield the experimentally observed mode behavior of the phonons.[20] This further confirms that the somewhat simpler but, at first sight, more universally applicable models of Chang and Mitra or of Lucovsky et al. fail, at least for some crystal structures, in predicting the correct mode behavior. The reason is not only that those models solely rely on the differences between the properties of the host atom and substituting atom but also that the vibrational patterns of the diatomic chain do not match those of binary host crystal structures with more than two atoms per primitive unit cell. It is also worth noting that Chaput et al. observe a strong resonance at low wavenumbers of about $70\ cm^{-1}$ due to the Sn impurity in a phonon density of states of $Mg_2Si_{31/32}Sn_{1/32}$ calculated by ab initio theory using supercells.[12] Unfortunately, this range is not accessible to us in the Raman experiments due to the constraints of the experimental setup. However, it would be interesting to see whether this resonance may be associated with an impurity-induced gap mode.

In this work, we studied the Raman-active modes of $Mg_2Si_{1-x}Sn_x$ as a function of composition x and observed a one-mode behavior for F_{2g} as well as for the F_{1u}(LO) mode. Both mode frequencies exhibit a linear variation with x, which

may prove useful for determining the composition of members of this solid solution. A comparison with theoretical predictions is rather difficult. On the one hand, the existing empirical models fail because there are more than two atoms in the primitive unit cell of the antifluorite structure. On the other hand, detailed ab initio calculations of the phonon structure of this solid solution are still lacking. This further emphasizes the importance of our investigation as modifications of the phonon structure due to alloying determine the phonon transport in solid solutions. A better understanding of the phonon structure of $Mg_2Si_{1-x}Sn_x$ is mandatory for the successful optimization of this solid-solution system for applications in thermoelectric devices.

Experimental Section

The $Mg_2Si_{1-x}Sn_x$ samples were synthesized by mechanical alloying using a high-energy ball mill (SPEX 8000D Shaker Mill) and a direct-current sintering press (DSP 510 SE) from Dr. Fritsch GmbH, Fellbach, Germany.[1b,21] Sintering at a holding temperature in the range between 600 and 800 °C for 10–60 min yielded pellets of homogeneous $Mg_2Si_{1-x}Sn_x$ phases of high purity with $x = 0$, 0.15, 0.2, 0.4, 0.5, 0.6, 0.7, 0.8, 0.9, and 1.0. Details of the sintering conditions of the $Mg_2Si_{1-x}Sn_x$ samples are given in **Table 1**.

The optimum sintering parameters (temperature and time) varied from sample to sample with different x, to form a homogenous uniform phase for each of the individual samples while sintering. Remnant inhomogeneity (Si-rich compositions) from the ball-milling step in samples with different x required different temperatures and holding durations to dissolve into the matrix by interdiffusion to form a uniform material. Details on homogenization of, e.g., for a $Mg_2Si_{0.5}Sn_{0.5}$ matrix and investigation of its microstructure by scanning electron microscope (SEM) can be found in our previous work.[21a,22] Furthermore, Sn-rich samples were less stable against Mg loss at high temperatures than Si-rich samples.[23] Therefore, to avoid Mg loss and formation of elemental impurities as well as to tune the microstructure, the sintering temperatures and durations were optimized for different compositions, from 600 °C for $x = 1$ (Mg_2Sn) to 800 °C for $x = 0$ (Mg_2Si). The conditions for the sample with $x = 0.2$ were an exception from this rule.

X-ray diffraction patterns were recorded of the sintered $Mg_2Si_{1-x}Sn_x$ pellets using either a Siemens D5000 Bragg–Brentano diffractometer with a secondary monochromator or a Bruker D8-Advance diffractometer. Cu Kα radiation (1.5406 Å) was used and the 2θ range between 20° and 80° was scanned with a step size of 0.01°.

The Raman spectra of all samples were obtained at room temperature using a Renishaw inVia Raman microscope system equipped with a holographic notch filter for suppression of the Rayleigh scattered light and a single spectrometer for dispersing the Raman-scattered light. A liquid nitrogen-cooled charge-coupled device detector was used for detection and an argon-ion laser operating at 514.5 nm for excitation. Raman spectra were taken with 10 s acquisition time and with a laser power of about 1 mW (with 10% of the maximum laser power) on the sample. The laser spot on the sample surface was about 1 μm in diameter. For each of the $Mg_2Si_{1-x}Sn_x$ samples, several Raman spectra (typically 5–13) were taken on different spots on the sample to check for sample homogeneity and consistency of the obtained data.

Table 1. Sintering conditions of $Mg_2Si_{1-x}Sn_x$ samples with $x = 0$ to 1 (after ball milling for 10–20 h).

x	0.0	0.15	0.2	0.4	0.5	0.6	0.7	0.8	0.9	1.0
Sintering temperature [°C]	800	700	750	700	700	700	700	650	650	600
Sintering duration [min]	10	60	10	60	60	60	60	60	30	10

Acknowledgements

Financial support is provided by the DFG via the GRK (Research Training Group) 2204 "Substitute Materials for sustainable Energy Technologies." The authors from DLR would like to acknowledge the endorsement from the DLR Executive Board Member for Space Research and Technology and financial support from the Young Research Group Leader Program. Financial support of H.K. is provided by the DAAD. Also, one of the authors (J.dB.) is partially funded by Deutsche Forschungsgemeinschaft (DFG, German Research Foundation), project number 396709363.

Conflict of Interest

The authors declare no conflict of interest.

Keywords

magnesium tin silicide, optical phonons, Raman spectroscopy, solid solutions, thermoelectric

Received: October 3, 2019
Revised: December 15, 2019
Published online:

[1] a) N. Farahi, S. Prabhudev, G. A. Botton, J. R. Salvador, H. Kleinke, *ACS Appl. Mater. Interfaces* **2016**, *8*, 34431; b) A. Sankhla, A. Patil, H. Kamila, M. Yasseri, N. Farahi, E. Mueller, J. de Boor, *ACS Appl. Energy Mater.* **2018**, *1*, 531; c) V. K. Zaitsev, M. I. Fedorov, E. A. Gurieva, I. S. Eremin, P. P. Konstantinov, A. Y. Samunin, M. V. Vedernikov, *Phys. Rev. B* **2006**, *74*, 045207; d) J. de Boor, T. Dasgupta, U. Saparamadu, E. Müller, Z. F. Ren, *Mater. Today Energy* **2017**, *4*, 105.
[2] G. J. Snyder, E. S. Toberer, *Nat. Mater.* **2008**, *7*, 105.
[3] C. Kittel, P. McEuen, *Introduction to Solid State Physics*, Wiley, New York **1996**.
[4] X. J. Tan, G. Q. Liu, H. Z. Shao, J. T. Xu, B. Yu, H. C. Jiang, J. Jiang, *Appl. Phys. Lett.* **2017**, *110*, 143903.
[5] P. Mooney, F. Dacol, J. Tsang, J. Chu, *Appl. Phys. Lett.* **1993**, *62*, 2069.
[6] F. Gather, A. Kronenberger, D. Hartung, M. Becker, A. Polity, P. Klar, B. Meyer, *Appl. Phys. Lett.* **2013**, *103*, 082115.
[7] a) R. L. Bjork, *Phys. Rev.* **1957**, *105*, 456; b) I. F. Chang, S. S. Mitra, *Phys. Rev.* **1968**, *172*, 924; c) G. Lucovsky, M. Brodsky, E. Burstein, *Phys. Rev. B* **1970**, *2*, 3295.
[8] S. de Gironcoli, S. Baroni, *Phys. Rev. Lett.* **1992**, *69*, 1959.
[9] a) P. Pandit, S. P. Sanyal, *Ind. J. Pure Appl. Phys.* **2011**, *49*, 692; b) J.-I. Tani, H. Kido, *Comput. Mater. Sci.* **2008**, *42*, 531; c) P. Baranek, J. Schamps, I. Noiret, *J. Phys. Chem. B* **1997**, *101*, 9147.
[10] a) C. Buchenauer, M. Cardona, *Phys. Rev. B* **1971**, *3*, 2504; b) S. Onari, M. Cardona, *Phys. Rev. B* **1976**, *14*, 3520; c) W. Whitten, P. Chung, G. Danielson, *J. Phys. Chem. Solids* **1965**, *26*, 49; d) R. Kearney, T. Worlton, R. Schmunk, *J. Phys. Chem. Solids* **1970**, *31*, 1085; e) T. H. Stuchlikova, V. Pic, M. Ledinský, A. Purkrt, Z. Remes, J. Stuchlik, *JJAP Conf. Proc.* **2017**, *5*, 011303.
[11] a) M. Hutchings, T. W. D. Farley, M. Hackett, W. Hayes, S. Hull, U. Steigenberger, *Solid State Ionics* **1988**, *28*, 1208; b) D. Bessas, R. Simon, K. Friese, M. Koza, R. Hermann, *J. Phys.: Condens. Matter* **2014**, *26*, 485401.
[12] L. Chaput, J. Bourgeois, A. Prytuliak, M. M. Koza, H. Scherrer, *Phys. Rev. B* **2015**, *91*, 064304.

[13] a) A. Kozlov, J. Gröbner, R. Schmid-Fetzer, *J. Alloys Compd.* **2011**, *509*, 3326; b) S. Vivès, P. Bellanger, S. Gorsse, C. Wei, Q. Zhang, J.-C. Zhao, *Chem. Mater.* **2014**, *26*, 4334.
[14] M. Cardona, in *Light Scattering in Solids II: Basic Concepts and Instrumentation* (Eds: M. Cardona, G. Güntherodt), Springer-Verlag, Berlin, Heidelberg **1982**, p. 19, Ch. 2.
[15] D. McWilliams, D. W. Lynch, *Phys. Rev.* **1963**, *130*, 2248.
[16] R. Geick, W. Hakel, C. Perry, *Phys. Rev.* **1966**, *148*, 824.
[17] a) I. Kosacki, K. Hibner, A. Litvinchuk, M. Y. Valakh, *Solid State Commun.* **1986**, *57*, 729; b) W. Lacina, P. Pershan, *Phys. Rev. B* **1970**, *1*, 1765; c) H. Verleur, A. Barker Jr, *Phys. Rev.* **1967**, *164*, 1169.
[18] R. F. Wallis, *Localized Excitations in Solids*, Springer, Berlin/New York **2013**.
[19] S. Ganesan, R. Srinivasan, *Can. J. Phys.* **1962**, *40*, 74.
[20] E. P. Bertin, *Principles and Practice of X-Ray Spectrometric Analysis*, Vol. *4*, 2nd ed., Plenum Press, New York **1975**.
[21] a) M. Yasseri, N. Farahi, K. Kelm, E. Mueller, J. de Boor, *Materialia* **2018**, *2*, 98; b) H. Kamila, P. Sahu, A. Sankhla, M. Yasseri, H.-N. Pham, T. Dasgupta, E. Mueller, J. de Boor, *J. Mater. Chem. A* **2019**, *7*, 1045; c) H. Kamila, A. Sankhla, M. Yasseri, N. P. Hoang, N. Farahi, E. Mueller, J. de Boor, *Mater. Today: Proc.* **2019**, *8*, 546.
[22] M. Yasseri, A. Sankhla, H. Kamila, R. Orenstein, D. Y. N. Truong, N. Farahi, J. de Boor, E. Mueller, *Acta Mater.* **2020**, *185*, 80.
[23] G. K. Goyal, T. Dasgupta, *J. Electron. Mater.* **2018**, *47*, 2066.